Accepted Manuscript

Synthesis and photophysical properties of deuteration of pirfenidone

Qiuju Yin, Yujie Chen, Meng Zhou, Xiangsheng Jiang, Junjun Wu, Yang Sun

PII:	S1386-1425(18)30550-X
DOI:	doi:10.1016/j.saa.2018.06.016
Reference:	SAA 16175
To appear in:	*Spectrochimica Acta Part A: Molecular and Biomolecular Spectroscopy*
Received date:	23 April 2018
Revised date:	29 May 2018
Accepted date:	4 June 2018

Please cite this article as: Qiuju Yin, Yujie Chen, Meng Zhou, Xiangsheng Jiang, Junjun Wu, Yang Sun , Synthesis and photophysical properties of deuteration of pirfenidone. Saa (2017), doi:10.1016/j.saa.2018.06.016

Synthesis and photophysical properties of deuteration of pirfenidone

Qiuju Yin[a1], Yujie Chen[a1], Meng Zhou[a1], Xiangsheng Jiang[a], Junjun Wu[a], Yang Sun[a,b]*

[a] School of Food Science and Technology·School of Chemical Engineering, Hubei University of Arts and Science, No. 296 Longzhong Road, Xiangyang, Hubei 441053, China

[b] School of Life Sciences, Tsinghua University, Beijing 100084, China

Corresponding author email: sunyang@if.usp.br (Y. Sun),

[1] These authors are co-first author of this work

Abstract

In order to improve the metabolism of pirfenidone (5-methyl-1-phenylpyridin-2-one, PFD), the methyl-deuterated version of pirfenidone via the substitution of hydrogen (H) at C-5 by its isotope deuterium (D, 5D-PFD) was synthesized and its photophysical properties were investigated. The negative solvatochrom was observed in absorption and fluorescence spectra with increasing solvent polarity, which implied that intermolecular charge transfer (ICT) involved $n\rightarrow\pi^*$ transition for both of PFD and 5D-PFD. The ground state and excited state dipole moment was calculated as 5.30 D and 3.30 D for PFD, and 3.70 D and 2.18 D for 5D-PFD, respectively, which suggested the more polar nature of PFD in the ground state than that of excited state compared with 5D-PFD. Density functional theory (DFT) results demonstrated a significant propensity of ICT from the electron-donor, methyl and carbonyl group to the amine group as an electron donor. The binding of metal ions with PFD or 5D-PFD induced a red-shift of $\pi\rightarrow\pi^*$ transition and blue-shift of $n\rightarrow\pi^*$ transition, respectively, indicating that the pyridone ring showed more stability upon binding of unoccupied orbital of metal ions with lone-pair electron of oxygen atom and thus prompted the electronic distribution on phenyl unit. Upon addition of metal ions, the aromatic region presented the characteristic upfield shifts, and the resonance contributed by 3-H showed a significant downfield chemical shift/deshielding effect, indicating the deduced resonance of 3-H and the improved electron distribution of phenyl unit. The binding and docking of human serum albumin showed that the affinity of 5D-PFD with HSA was lower than that of PFD, and also 5D-PFD might prefer to present free forms in the blood with better efficacy comparing with PFD. The pharmacokinetic of half-time ($T_{1/2}$) for oral and *i.v.* administration of 5D-PFD was found around 19 and 30 min, higher than that of *i.v.* administration of PFD, 8.6 min, reported by Giri et al. [1]. The results of this work suggest that the deuteration enhances the metabolism of PFD significantly with little change of physical-chemical property.

Keywords: Pirfenidone; isotope deuterium; negative solvatochrom; density functional theory; metal ions; human serum albumin.

1. Introduction

Pirfenidone (PFD) is a widespread, universal antifibrotic pyridine ketone compound, chemical name is 5-methyl-1-phenyl-2-[1H]-pyridone, which possesses antifibrotic effects by regulating the key fibrotic cytokines and growth factors, inhibiting several inflammatory mediators, attenuating the fibroblast proliferation, differentiating related collagen synthesis, and restoring the immune response balance [2]. These beneficial effects of PFD inhibits progression of fibrosis in vivo in a variety of animal models of lung [3], kidney [4], hepatic [5] and cardiac fibrosis [6]. And PFD is used clinically for treating idiopathic pulmonary fibrosis [7]. However, PFD-induced phototoxicity occurred after oral administration as an adverse event in previous clinical trials [7] and animal model [8, 9]. According to Seto et al., a high dose of PFD (160 mg/kg) might cause phototoxic responses through the generation of ROS in the skin, and PFD is photoreactive, and the generation of ROS from UV-exposed PFD might lead to a photo-irritation risk, but not to photo-genotoxic potential [10].

The alteration of the oxidative metabolism of drug candidates to improve their pharmacokinetic or reduce the toxicological properties is important aspect of the drug discovery process. Since Belleau et al. [11] among the first reported the pharmacodynamic effect of deuteration with αα-dideuterated *p*-tyramine, there has been a burgeoning interest, particularly from intellectual property aspects, for enhancing the pharmacokinetic, pharmacodynamic, and reducing the toxicological properties of drug [12-14]. Deuteration of drugs to enhance their pharmacokinetic, pharmacodynamic, or toxicological properties has gained momentum as judged by a search of the SciFinder database with the search term “deuterated drugs”[15]. Although the deuteration would be benefit for clinical use of medicine, the photophysical and photochemical properties of deuterated compounds have not been fully elucidated, and also the mechanisms of deuterated compounds reducing phototoxicity are not clear, since the molecular structure mainly determines the activity of the compound [16]. Apart from substitution changes, solvent effect plays an important part in chemical and physical properties in solution [17]. The solvent-induced changes in the electronic transition of solutes, namely

solvatochromism, are helpful for understanding the solvent effects [18, 19].

So far, few studies have been reported the photophysical and photochemical properties of PFD and its derivatives. Therefore, in this work, the 5D-PFD was synthetized by replacing CH-5 as CD-5 in order to improve the metabolism of PFD, and its structure was characterized. Falb et al. have reported a Suzuki–Miyaura methylation of pyridines leading to the PFD, which focus on a green methylation route to avoid the environmental and economic impact of employing alkyllithium at cryogenic temperatures, simplifying the synthesis process and reducing the cost for synthesis [16]. In this work, besides the deuterated methyl of pyridone, the fluorine is introduced into phenyl ring in order to impede the oxidation rate of phenyl group and further improve the metabolism of PFD. Moreover, we propose a green reaction avoiding the use of the benzene solvent, prompting the environmental protection. The solvent effect of PFD and 5D-PFD was studied by absorption and fluorescence spectra, and the solvatochromic parameters were calculated according to the spectral data. Moreover, the density functional theory (DFT) provided the ground state properties of PFD and 5D-PFD, such as geometrical parameters, dipole moment and charge transfer. Beside these, the attempts were made to assess if there was any deuteration-induced difference in human serum albumin (HSA) binding with PFD and 5D-PFD, including binding site, binding energy and type of interaction force. These results would have a great significance in pharmacology and clinical medicine as well as methodology.

2. Experimental

2.1. Materials

5-Bromo-2-methylpyridine, n-Buli, MTBE (methyl tert-butyl ether), iodomethane-D3, were purchased from Aldrich. Stock solution of PFD and 5D-PFD (0.1 mM) was prepared by ethanol and kept in darkness. All the solvents were of analytic grade.

2.2. Methods

2.3.1. Synthesis of 5D-PFD

5-Bromo-2-methylpyridine (3.67 g) was dissolved in 10 m MTBE under a N_2 atmosphere with a temperature of -78°C. Then, 8.8 mL (2.5 M) n-Buli was added

dropwise over a period of 1.5 h. Thereafter, the resulting mixture was added by CD_3I dropwise between -60°C to -80 °C over 1.5 hours and then the mixture was warmed up to room temperature. After the completion of the reaction (monitored by TLC), the mixture was extracted by 6N HCl (30mL × 2) and the water phase was collected and then refluxed to react over 48 h (monitored by LC-MS). The reaction mixture was cooled to room temperature and gave a pH around 12, after that, the solution of above mixture was stirred at reflux for 24 h. LC-MS detected 65% reacted, another 24 h, LC-MS detected over 95% 5-bromo-2-methylpyridine consumed. After cooling to room temperature, the reaction mixture was filtered to isolate the resulting precipitate, which was then washed sequentially with toluene (40 mL × 2) and 40 mL water. Drying the organic phase and the solvent was evaporated under reduced pressure to give the residue, which was then purified through flash chromatography (DCM: MeOH=20: 1) to give a white solid, yield 71.3%, purity ≥ 98%. The synthetic route was listed in Fig. 1. m.p. 292–295 ºC.; IR (cm^{-1}): Need to add IR data and nuclear magnetic data3189 (νNH_2); 2831 (νCH); 1734 (νC=O);; 1245 (νC–O); 1131 (νC–O–C). ^{1}H NMR (500 MHz, DMSO-d_6) δ: 8.43 (d, *J* = 6.4 Hz, 1H), 8.10-7.93 (d, *J* = 5.1 Hz, 2H), 7.57 (t, *J* =7.3 Hz, 1H), 6.73 (d, *J* = 8.1 Hz, 1H), 4.11 (s, 2H), 3.75-3.86 (t, *J* = 9.2 Hz, 4H), 3.17 (s, 4H), 2.65-2.74 (t, *J* = 4H), 2.35 (s, 6H).

2.3.2. Molecular modeling and theoretical calculation

The crystal structure of HSA with resolution of 2.25 Å was obtained from the Protein Data Bank (PDB code: 2BXH). The docking scheme was summarized as follows. Firstly, the preprocessing of HSA was carried out by using the programs of Discovery Studio 2.5 (Accelrys, Inc., USA), which included removing water, adding hydrogen atoms and assigning CHARMM like force field. PFD and 5D-PFD were built and geometry optimized using SYBYL with convergent thresholds of 0.02Å. The molecular docking program GOLD3.2 was used for molecular docking studies and the binding site was defined as a sphere containing the residues that stay within 10 Å from ligand in this crystal structure. One hundred binding conformations were preserved for each ligand, and the docking software automatically determines the docking space based on the algorithm and automatically specifies the atomic type of

the ligand atom, and the remaining parameters are set as the default values. The optimized conformations were selected and the binding energy of ligands with two binding sites using the ACFIS online server (ACFIS: a web server for fragment-based drug discovery).

DFT calculations in the present study were performed by using the Amsterdam Density Functional package (ADF) 2009.01 program [20]. Geometry optimization in the ground state was carried out using B3LYP density functional calculations[21], with the DZP basis sets (all-electron double zeta plus polarization function) [22].

2.3. Apparatus

EQUINOX55 Fourier transformed infrared spectrometry (Bruker Company, Germany). AVANCF600 MHz digital superconducting NMR Fourier (Bruker Company, Germany). X-5 microscopic melting point apparatus (Tech Instrument Co., Ltd. Beijing, China). The absorption spectra were recorded by UV–vis ratio recording spectrophotometer (Hitachi model U-2501). The fluorescence measurements were carried out on an F-2700 fluorescence spectrometer (Hitachi, Japan) equipped with a 150W Xenon lamp. A 1.0 cm quartz cell was used for measurements. Elemental analysis data were obtained on a Perkin–Elmer 240c instrument.

2.2. Chromatographic Equipment and Conditions

The UHPLC analysis was performed with a Waters Acquity™ UPLC system (USA). Chromatographic separation was carried out at 40°C on an ACQUITY UPLC BEH C18 column 1.7 μm (2.1 × 50 mm,). The mobile phase consisted of 0.1% formic acid water solution (A) and 0.1% formic acid ACN solution (B). The optimized UHPLC elution conditions were: 0 min, 70% A-30% B, 0.4-0.8 min, 5% A-95% B; 0.81-1.2 min, 70% A-30% B. The autosampler was maintained at 4°C. The sample volume injected was 2.5 μL, the flow rate was 0.55 mL min^{-1}, and the detector wavelength was set at 310 nm. Data were acquired and processed with an Empower 2.0 chromatography data system. For UHPLC determination, calibration standards of 5D-PFD at concentration levels of 0.1, 0.2, 0.5, 1.0, 5.0, 8.0, 10.0 μM were prepare by spiking the appropriate amounts of the standard solutions into blank plasma obtained from healthy rats. The quality control (QC) samples were separately prepared in a

similar manner as those used for the calibration curves. The blood samples (approximately 200 μL) were collected from the ophthalmic vein in heparinized tubes at control and 1, 5, 10, 15, 20, 30, 40, 60, 150 and 300 min after oral or *i.v.* administration. Samples were immediately centrifuged at 6000 *g* for 10 min and the plasma was frozen at -25°C and stored until analysis according to our previously described method [23]. Pharmacokinetics analysis was carried out by a non-compartmental method with the aid of DAS 2.0 software.

3. Results and discussion

3.1. Solvent effect on spectra of PFD and 5D-PFD

The optimized ground-state geometries of PFD and 5D-PFD were confirmed to be minimum-energy conformations using ADF program at B3LYP–DZP level, as shown in Fig.2, the pyridine ring substituents are coplanar and the phenyl group is found to be almost perpendicular with pyridone ring. This perpendicular structure would be unfavorable because it hinders charge transfer from the donor, pyridone group, to acceptor unit, phenyl ring. As expected, there is little conformation difference between PFD and 5D-PFD. The weak π-conjugation effect probably contributes to the non-stability of PFD, and the ROS generation from PFD exposes to UV radiation, which may potentially cause photochemical reactions and lead phototoxic skin responses [10]. An important experimental technique for probing solute-solvent interactions is the solvent dependence of the absorption and fluorescence spectra, in which the different electronic properties (multipole moments, polarizabilities, etc.) of the ground and excited state lead to a shift in the electronic excitation energy or spectra, and this shift is a direct measure of the specific interactions of solute-solvent [24].

The absorption and fluorescence spectra of PFD and 5D-PFD in different solvents were shown in Fig. 2, and the corresponding values of wavenumber of maximum absorbance and emission were listed in Table1. As seen from Figs. 2A and 2C, the absorption maximum of PFD in water and hexane is 311 nm and 334 nm, and the absorption maximum of 5D-PFD in water and hexane is 314 nm and 327 nm,

respectively. Meantime, the fluorescence spectra in different solvents (Figs. 2B and 2D) show that as the solvent polarity increases (hexane to water), the emission of PFD shifts from 409 to 391 nm (hypsochromic shift) and emission of 5D-PFD in water and hexane is 404 nm and 390 nm, respectively. The hypsochromic shift happens when the dipole moment of the compound decreases during the electronic transition i.e., the dipole moment of ground state S_0 is higher compared to that in the excited state S_1 ($\mu_e > \mu_g$), in which the S_0 state is energetically stabilized relative to the relaxed S_1 state and the S_0 state is formed in solvent cage of already partly oriented solvent molecules, consequently, thus a significant hypsochromic shift of the spectra is observed.

Moreover, the Stokes shift of PDF in hexane is 57 nm, whereas the Stokes shift in water increases to 98 nm, and the Stokes shift of 5D-PDF in hexane is 63 nm, while the Stokes shift in water is 90 nm, respectively. The increased Stokes shift in polar protic solvents suggests that PFD and 5D-PFD may present the feature of the intramolecular charge transfer (ICT), and the weak intermolecular hydrogen bonding of carbonyl group with protic solvents may induce electron distributions. One group of chromophores containing carbonyl group have characteristically weak n→π* absorption bands [25]. For an n→π* electronic excitation, when one strong localized electron in an n orbital goes to a more delocalized π* orbital, leads a meaningful reduction of the dipole moment, and a labile lone-pair in the system provides electronic donor properties. Therefore, it fosters hydrogen bonding with protic solvents, which induces an energy stabilization of the lone-pair, and be larger in the ground state than in the n→π* excited state, thereby blue-shift of transition is observed [26]. In the n→π* transition in pyridone, an ICT occurs from the carbonyl oxygen lone-pair into the antibonding π* orbital, localizing above and beneath the plane spanned by the carbonyl group. This excitation leads to a reduction of the dipole moment of PFD and 5D-PFD and consequently, a different solvation of the electronic ground and excited states occurs. Since the dipole moment has a decreased magnitude in the n→π* S_1 state as compared to the S_0 state, PFD or 5D-PFD is more favorably stabilized in the S_1 state through intermolecular hydrogen bonding interactions of

oxygen atom with protic solvent. Solvatochromic shifts of dependent the electronic absorption spectra of molecules, solvent polarity scales have been established including the popular E_T^N scale based on Reichardt's betaine dye [27, 28]. In order to investigate the main type of interaction of PDF or 5D-PFD with solvents, the multiple regression approaches based on solvatochromic equations were used and the Onsager model was taken into consideration:

Lippert-Mataga equation [29]:

$$\nu_a - \nu_f = m_{Lippert\text{-}Mataga} F_{Lippert\text{-}Mataga}(\varepsilon, n) + \text{constant} \quad (1)$$

Bakhshiev's equation[30]:

$$\nu_a - \nu_f = m_{Bakhshiev} F_{Bakhshiev}(\varepsilon, n) + \text{constant} \quad (2)$$

Kawski-Chamma-Viallet's equation[31, 32]:

$$(\nu_a + \nu_f)/2 = m_{Kawski\text{-}Chamma\text{-}Viallet} F_{Kawski\text{-}Chamma\text{-}Viallet}(\varepsilon, n) + \text{constant} \quad (3)$$

McRae's equation [33]:

$$\nu_a = -m_{McRae} F_{McRae}(\varepsilon) + \text{constant} \quad (4)$$

Suppan's equation [34]:

$$\nu_a = -m_{Suppan} F_{Suppan}(\varepsilon) + \text{constant} \quad (5)$$

where *va* and ν_f is the wavenumber of the absorption and emission maxima respectively, the symbol *h* and *c* are Planck's constant and the velocity of light in vacuum, respectively. $F_{Lippert–Mataga}$, $F_{Bakhshiev}$, $F_{Kawski–Chamma–Viallet}$, F_{McRae} and F_{Suppan} are solvent polarity functions and given as:

$$F_{L-M}(\varepsilon, n) = \frac{\varepsilon - 1}{2\varepsilon + 1} - \frac{n^2 - 1}{2n^2 + 1} \quad (6)$$

$$F_B(\varepsilon, n) = \frac{2n^2 + 1}{n^2 + 2}\left[\frac{\varepsilon - 1}{\varepsilon + 2} - \frac{n^2 - 1}{n^2 + 2}\right] \quad (7)$$

$$F_{K-C-V}(\varepsilon, n) = \left[\frac{2n^2 + 1}{2(n^2 + 2)}\left(\frac{\varepsilon - 1}{\varepsilon + 2} - \frac{n^2 - 1}{n^2 + 2}\right) + \frac{3(n^4 - 1)}{2(n^2 + 2)^2}\right] \quad (8)$$

$$F_M(\varepsilon) = \frac{2(\varepsilon - 1)}{\varepsilon + 2} \tag{9}$$

$$F_S(\varepsilon) = \frac{2(\varepsilon - 1)}{2\varepsilon + 1} \tag{10}$$

$$g(n) = \frac{3}{2}\left(\frac{n^4 - 1}{(n^2 + 2)^2}\right) \tag{11}$$

$$\varphi(\varepsilon, n) = F_B(\varepsilon, n) + 2g(n) \tag{12}$$

$g(n)$ is the solvent polarity parameter, and the symbol ε and n is dielectric constant and refractive index of the solvent, respectively. The fitting of linear curve of ν_a - ν_f vs $F_{Lippert–Mataga}$, ν_a - ν_f vs $F_{Bakhshiev}$, (ν_a + ν_f)/2 vs $F_{Kawski–Chamma–Viallet}$, ν_a vs F_{McRae} and ν_a vs F_{Suppan} gives the slope of $m_{L–P}$, m_B, $m_{K–C–V}$, m_B and m_S, respectively, and is given as:

$$m_{L-M} = 2(\mu_g - \mu_{e\,(L-M)})^2 / hca_0^3 \tag{13}$$

$$m_B = 2(\mu_g - \mu_{e(B)})^2 / hca_0^3 \tag{14}$$

$$m_{K-C-V} = 2(\mu_g^2 - \mu_{e\,(K-C-V)}^2) / hca_0^3 \tag{15}$$

$$m_M = \frac{\mu_g(\mu_g - \mu_{e(M)})}{hca_0^3} \tag{16}$$

$$m_S = \frac{\mu_g(\mu_g - \mu_{e(S)})}{hca_0^3} \tag{17}$$

where μ_g is the ground state dipole moment, μ_e(L-M), μ_e(K-C-V), μ_e(M) and μ_e(S) is the excited state dipole moment from the correlation of Lippert–Mataga, Bakhshiev, Kawski–Chamma–Viallet, McRae and Suppan, respectively. The parameter m_{L-M}, m_B, m_{K-C-V}, m_M and m_S can be calculated from Eqs. (1)-(5). The symbol '*a*' is the Onsager radius of the solute molecule, with the values evaluated by using atomic increment method [35]. If it can be supposed that ground and excited state dipole moment are parallel, then:

$$\mu_g = \frac{m_{K-C-V} - m_B}{2}\left(\frac{hca_0^3}{2m_B}\right)^{1/2} \tag{18}$$

$$\mu_e = \frac{m_{K-C-V} + m_B}{2}\left(\frac{hcq_0^3}{2m_B}\right)^{1/2} \quad (19)$$

$$\mu_e / \mu_g = \frac{m_{K-C-V} + m_B}{m_{K-C-V} - m_B} \ (m_{K\text{-}C\text{-}V} > m_B) \quad (20)$$

The normalized value of E_T^N, based on the empirical polarity scale, is used for estimating dipole moment difference ($\Delta\mu$) from solvatochromic shift [36, 37], correlating the effect of polarity of solvent and also the effect of protic hydrogen bonding on the spectral shift [38],

$$\nu_a - \nu_f = 11307.6\left[\left(\frac{\Delta\mu}{\Delta\mu_B}\right)^2\left(\frac{a_B}{a_0}\right)^3\right]E_T^N + \text{constant} \quad (21)$$

where $\Delta\mu_B$=9 D and a_B=6.2 Å are the dipole moment difference of excitation and Onsager radius of reference betaine dye, respectively. The symbol a_0 is the Onsager radius for the solute molecule, which indicated as:

$$a_0 = \left(\frac{3M}{4\pi\delta N}\right)^{1/3} \quad (22)$$

where N is the Avogadro's number, M is the solute's molecular weight and δ is the solid-state density of solute. For PFD and 5D-PFD, δ is 1.146 g/cm^3 and 1.198 g/cm^3 with M of 185.22 g/mol and 205.22 g/mol and thus, a_0 of PFD and 5D-PFD is 4.01 Å and 4.08 Å.

The $\Delta\mu$ can be evaluated from the slope of Stokes shift *vs* E_T^N plot and is given by the equation can be determined as [39, 40]:

$$m_{E_T^N} = 11307.6\left[\left(\frac{\Delta\mu}{\Delta\mu_B}\right)^2\left(\frac{a_B}{a}\right)^3\right] \quad (23)$$

E_T^N is defined using water and tetramethylsilane (TMS) as extreme reference solvents with an equation:

$$E_T^N = \frac{E_T(solvent) - E_T(TMS)}{E_T(water) - E_T(TMS)} = \frac{E_T(solvent) - 30.7}{32.4} \quad (24)$$

$$E_T(solvent) = hcN\nu_a = 2.8591\times10^{-3}\nu_a$$

where ν_a (cm^{-1}) is the absorption maxima of the standard betaine dye in solvent.

Therefore, the difference of dipole moment is obtained from:

$$\Delta\mu = \mu_g - \mu_e = \sqrt{\frac{m_{E_T^N}}{1.707a_0^3}} \quad (25)$$

where, $m_{ET}{}^N$ is the slope of the linear curve of Stokes shift vs $E_T{}^N$, obtained from Eq. (21).

The plots of Stokes shift (v_a-v_f and v_a+v_f) versus solvatochromic parameters ($f(\varepsilon, n)$ and $f(\varepsilon, n) + 2g(n)$) and $E_T{}^N$ were listed in Fig. 3, and the results of dipole moment of PFD and 5D-PFD were listed in table 3. One can see that the μ_g and μ_e of PFD is 5.30 D and 3.30 D, and the μ_g and μ_e of 5D-PFD is 3.70 D and 2.18 D, which is agreement the results of energy transition mentioned above. The dipole moments of PFD in S_0 and S_1 are higher than that of 5D-PFD, suggesting the more polar nature of PFD in the ground state than that of excited state compared with 5D-PFD. The time-dependent density functional theory (TD-DFT) [41] was used to verify the results of dipole moment of compounds, and the values of μ_g and μ_e for PFD is 7.41 D and 5.44 D, and values of μ_g and μ_e for 5D-PFD is 4.77 D and 3.10 D. The values calculated by TD-DFT are larger than that of calculated by solvatochromic method, since the calculation of TD-DFT is processed in gas phase, and also the practical function and solvent effect is not considered. This result may imply that the ground state energy distribution is not affected to a greater extent possibly due to the more polar nature of the drug in the ground state than in excited state. Similar negative solvatochromism behavior has been reported in some articles [41, 42].

The absorption spectra of organic molecules are induced by electron transfers from ground state to excited state after absorbs energy, and the maximum absorption wavelength electronic transition is from HOMO (highest occupied molecular orbital) to LUMO (lowest unoccupied molecular orbital). In order to obtain more insight into the electronic distribution of PFD and 5D-PFD, the density functional theory (DFT) calculations has been performed. As seen from Fig. 5, the HOMO or LUMO of PFD and 5D-PFD corresponding to the n→π* transition mentioned above shows similarity,

the charge distributes around methyl and carbonyl group acting as an electron donor for HOMO, and the charge transfer to phenyl group and mainly locates at amine unit contributing to the electron withdrawing effect of amine in the case of LUMO. These indicate that the deuteration shows few effects on the charge transition property, and the significant ICT characteristic of electron immigration from methyl group to phenyl group is found for both of PFD and 5D-PFD.

Effect of metal ions on the absorption and NMR spectra

As seen from Figs. 6A and 6B, the absorption of PFD or 5D-PFD presents two bands, the shorter wavelength at range of 200-250 nm originated from the π→π* transition of phenyl group, the longer wavelength at range of 300-360 nm contributed by n→π* transition (HOMO−LUMO) as mentioned above. With addition of metal ions (Ag^{+}, Al^{3+}, Cu^{2+}, Fe^{3+}, K^{+}, Mg^{2+}, Pb^{2+} and Zn^{2+}), PFD and 5D-PFD show similar spectral change, the slight blue-shift of 325 nm absorption band, but significant red-shift of 225 nm 225 nm band, suggesting that the pyridone ring shows more stability upon binding of unoccupied orbital of metal ions with lone-pair electron of oxygen atom. This prompts the electronic distribution on phenyl group and thus decreases the stability of phenyl group. The effects of metal ions (Ag^{+}, Al^{3+}, Cu^{2+}, Fe^{3+}, K^{+}, Mg^{2+}, Pb^{2+} and Zn^{2+}) on the ^{1}H NMR spectra of PFD and 5D-PFD were investigated and the results were shown in Figs. 6C-6F, and the Fe^{3+} ion was excluded since its paramagnetic effect. The resonance from 7.55 ppm to 7.30 ppm is contributed by protons of phenyl group, and this region shows the characteristic upfield shifts with addition of metal ions, suggesting that the binding of metal ions improves the π-π* transition thus prompts the electron density of phenyl group. And the resonance from 6.42 ppm to 6.42 ppm contributed by 3-H shows a strong downfield chemical shifts/deshielding effect upon metal binding, which indicates that the binding of unoccupied orbital of metal ions with lone-pair electron of oxygen atom presents the electron withdrawing effect, and thus deduces the energy of 3-H, which is agreement with the results of absorption spectra.

Analysis of binding ability of human serum albumin and the pharmacokinetic

Human serum albumin (HSA) is an important protein in plasma, it can not only transport fatty acids, pigments, steroid hormones, metal ions and other important physiological active substances, but also carry many drug molecules. HSA also plays a decisive role in some pharmacological properties of drugs (practical aspects of the ligand-binding and enzymatic properties of HSA). HSA has seven ligand binding pockets, while the Drug site 1 and Drug site 2 is the major drug binding pocket.

The effects of PFD and 5D-PFD on the fluorescence spectra of HSA have been investigated in order to elucidate the binding mechanism. As shown in Figs. 7A and 7B, the fluorescence intensity of HSA decreases regularly with little shit of emission upon increasing concentrations of PFD or 5D-PFD, and the maximum emission of both PFD and 5D-PFD are around 397 nm with the excitation wavelength of 280 nm. The fluorescence quenching is usually described by the Stern–Volmer equation [19]:

$$F_0/F=1+K_{sv}[L]=1+K_q\tau_0[L] \quad (27)$$

where F_0 and F is the fluorescence intensity in the absence and presence of ligand (PFD or 5D-PFD), K_{sv} is the Stern–Volmer quenching constant and [L] is the ligand concentration, K_q is the biomacromolecule quenching rate constant and τ_0 is the average lifetime biomacromolecule, usually as 10^{-8} s [8]. The binding constant (K_a) was calculated following as:

$$\log(F_0-F)/F=\log K_a + n \log[L] \quad (28)$$

where, n is the number of binding sites and F_0, F and [L] have the same meaning as in Eq. (27).

As seen from Figs. 7C and 7D, the value of K_a for PFD-HSA and 5D-PFD-HSA is 0.67 μM^{-1} and 0.41 μM^{-1}, and corresponding value of n is 1.75 and 1.20, respectively. This indicates that the affinity of 5D-PFD with HSA is lower than that of PFD, and

also 5D-PFD may prefer to present free forms in the blood with better efficacy comparing with PFD, despite the slight difference of binding parameters between two ligands with HSA.

In order to investigate the binding mechanism of PFD or 5D-PFD with HSA, the molecular docking using GOLD program has been employed by situating PFD or 5D-PFD within sub-domain IIA hydrophobic cavity of HSA, site I and site II, respectively. As shown in Figs. 8A and 8B, for both of PFD and 5D-PFD, the phenyl group is found to be almost coplanar with pyridone ring in the site I, and the oxygen atom of carbonyl group forms the significant hydrogen bonding with G196 and pyridone ring contacts with Trp214 and Lys199 by Van de Waal and hydrophobic interaction. The phenyl group is adjacent to K199 with considerable π-π interaction, and the hydrophobic interactions of H242, A291, V238 and Y150 with PFD also promote the matching of ligand with active cavity. On the other hand, as seen from Fig. 8C, two aromatic rings of PFD are close to be perpendicular inside of site II, carbonyl group forms two hydrogen bonds with R410 meantime, and the van de waals and hydrophobic interaction play key role in connecting of pyridone ring with Y441 and L457. The phenyl group inserts the hydrophobic cavity formed by L407, L430, L453, L387, V433 and F403, which is contributed mainly by hydrophobic interaction. Moreover, as shown in Figs. 8B and 8D, the 5D-PFD presents little difference of binding model with HSA comparing with native one. The result of docking suggests that PFD and 5D-PFD show the similar binding model and mechanism. However, GOLD program can't provide the energy information about binding, thus, the MM_PBSA method of AMBER8 program to calculate the binding energy of PFD and 5D-PFD with HSA [43]. As seen from Table 4, the ΔG_{PB} of site II is higher than that of site I and the value of ΔG_{PB} of 5D-PFD is slight lower than that of PFD, indicating that ligands could form hydrophobic and van de waals interaction inside of site II and dominate the binding, and also the infinity of 5D-PFD with HSA is lower than that of PFD, which is agreement with the spectral results.

Moreover, the pharmacokinetics of 5D-PFD has been evaluated after oral (20 mg kg^{-1}) and *i.v.* (5 mg kg^{-1}) administration into normal rats by the method of the previous report [44], and the time course plasma levels is listed in Fig. 9 and pharmacokinetic parameters are summarized in Table 5. Plasma levels of 5D-PFD present a peak around 25 min for oral administration and plasma levels of 5D-PFD fall significantly in a biexponential fashion for *i.v.* administration (Fig. 9). The $T_{1/2}$ value oral and *i.v.* administration of 5D-PFD is around 19 and 30 min, higher than the $T_{1/2}$ value of *i.v.* administration of PFD, 8.6 min, reported by Giri et al. [1], which suggests that the deuteration enhances the pharmacokinetic of PFD significantly with little change of physical-chemical properties. And the enhanced metabolism and pharmacokinetic of 5D-PFD in rat clearly underscores the need for appropriate kinetic studies in humans.

4. Conclusion

PFD has shown anti-inflammatory and anti-fibrotic properties and suppressed the progression of fibrotic and inflammatory, however, the rapid metabolism and clearance restrains the further clinical application of PFD. Thus, in this work, in order to improve the metabolism of PFD, 5D-PFD has been synthesized by substituted hydrogen at C-5 with its isotope deuterium (D), and the photophysical properties have been investigated. For both of PFD and 5D-PFD, the ICT involves $n\rightarrow\pi^*$ transition from the electron-donor methyl and carbonyl group to the amine group acting as an electron withdrawing effect. The diploe moment calculation results suggest that PFD shows a more polarity in the ground state than excited state compared with 5D-PFD. The binding of metal ions with PFD or 5D-PFD improves the stability of pyridone ring due to the binding of unoccupied orbital of metal ions with lone-pair electron of oxygen atom. The binding and docking of HSA results demonstrate that the affinity of 5D-PFD with HSA is lower than that of PFD, and also 5D-PFD may prefer to present free forms in the blood with better efficacy comparing with PFD, despite the little different binding energy and site of two ligands with HSA. The pharmacokinetic of $T_{1/2}$ values by oral and *i.v.* administration of 5D-PFD is found around 19 and 30 min, which is almost 4 times than that of value reported by Giri et al. [1]. The experimental and theoretical results offer a rationale for understanding the photophysical properties of PFD and its deuterium derivates, 5D-PFD, which would be available for wider clinical application of PFD as active drug.

Acknowledgement

This work is supported by the Natural Science Foundation of Hubei Province (2016CFB317) and the Doctoral Initiate Foundation of Hubei University of Arts and Science.

Table 1. Absorption (v_a) and fluorescence (v_f) spectral wavelengths for PFD and 5D-PFD (described in cm^{-1})

Solvents	PFD					5D-PFD				
	v_a	v_f	v_a-v_f	(v_a+v_f)	(v_a+v_f)/2	v_a	v_f	v_a-v_f	(v_a+v_f)	(v_a+v_f)/2
water	32154.34	25575.45	6578.89	57729.79	28864.89	31847.13	25641.03	6206.11	57488.16	28744.08
Acetonitrile	31055.90	25188.92	5866.98	56244.82	28122.41	31152.65	25000	6152.65	56152.65	28076.32
DMF	31043.76	25143.54	5900.22	56187.3	28093.65	31112.76	24981.54	6131.22	56094.3	28047.15
Methanol	31847.13	25445.29	6401.84	57292.42	28646.21	31645.57	25380.71	6264.86	57026.28	28513.14
Ethanol	31545.74	25000	6545.74	56545.74	28272.87	31438.92	25316.46	6229.29	56862.2	28431.1
Acetone	31003.42	24901.31	6102.11	55904.73	27952.365	31086.14	24832.52	6253.62	55918.66	27959.33
n-Butanol	31347.96	24937.66	6410.3	56285.62	28142.81	31347.96	25125.63	6222.33	56473.59	28236.8
Ethyl acetate	30674.85	24813.98	5860.87	55488.83	27744.415	31055.9	24937.66	6118.24	55993.56	27996.78
Chloroform	30487.81	24691.36	5796.45	55179.17	27589.585	30864.2	24875.62	5988.58	55739.82	27869.91
Toluene	30211.48	24509.81	5701.67	54721.29	27360.645	30674.85	24813.9	5860.95	55488.74	27744.37
Benzene	30193.72	24494.23	5699.49	54687.95	27343.975	30637.19	24772.36	5864.83	55409.55	27704.78
Cyclohexane	30112.13	24462.69	5649.44	54574.82	27287.41	30602.24	24761.73	5840.51	55363.97	27681.99
n-Hexane	29940.12	24449.88	5490.24	54390	27195	30581.04	24752.48	5828.56	55333.52	27666.76

Table 2 Solvatochromic parameters

Solvents	ε	N	α	β	$\varphi(\varepsilon, n)$[a]	$g(n)$	$F_{L\text{-}M}(\varepsilon, n)$	$F_B(\varepsilon, n)$[b]	$F_{K\text{-}C\text{-}V}(\varepsilon, n)$	$F_M(\varepsilon)$	$F_S(\varepsilon)$	E_T^N
water	80.40	1.331	1.17	0.47	1.3653	0.2255	0.3209	0.9143	0.6826	1.9272	0.9815	1.000
Acetonitrile	38.01	1.344	0.19	0.40	1.3328	0.2343	0.3057	0.8643	0.6664	1.8500	0.9610	0.460
DMF	36.71	1.431	0.00	0.69	1.4201	0.2924	0.2742	0.8354	0.7101	1.8450	0.9597	0.386
Methanol	33.71	1.328	0.98	0.66	1.3047	0.2235	0.3094	0.8578	0.6523	1.8320	0.9562	0.762
Ethanol	24.55	1.361	0.86	0.75	1.3045	0.2457	0.2889	0.8131	0.6523	1.7740	0.9401	0.654
Acetone	20.56	1.359	0.08	0.48	1.2780	0.2444	0.2840	0.7893	0.6390	1.7340	0.9288	0.355
n-Butanol	17.40	1.399	0.84	0.84	1.2917	0.2711	0.2633	0.7494	0.6459	1.6907	0.9162	0.241
Ethyl acetate	6.02	1.372	0.00	0.45	0.9955	0.2531	0.1998	0.4893	0.4977	1.2519	0.7699	0.228
Chloroform	4.81	1.446	0.20	0.10	0.9753	0.3022	0.1482	0.3709	0.4877	1.1189	0.7175	0.259
Toluene	2.38	1.497	0.00	0.11	0.6999	0.3354	0.0132	0.0290	0.3499	0.6301	0.4792	0.099
Benzene	2.27	1.559	0.00	0.10	0.7163	0.3750	-0.0148	-0.0337	0.3582	0.5948	0.4585	0.111
Cyclohexane	2.02	1.427	0	0	0.5756	0.2897	-0.0019	-0.0038	0.2878	0.5075	0.4048	0.164
n-Hexane	1.88	1.375	0	0	0.5076	0.2551	-0.0014	-0.0026	0.2538	0.4536	0.3697	0.009

[a] $\varphi(\varepsilon, n)$= f (ε, n)+2g(n)

[b] $F_B(\varepsilon, n)$=f (ε, n)

Table 3 Calculated parameters according spectral data of PFD and 5D-PFD in solvents.

Compound	Equation	Intercept	Slope	*R*	Onsager radius (Å)	μ_g[b]	μ_e[c]	$\mu_{e(L\text{-}M)}$[d]	$\mu_{e(B)}$[e]	$\mu_{e(K\text{-}C\text{-}V)}$[f]	$\mu_{e(M)}$[g]	$\mu_{e(S)}$[h]	μ_e/μ[j]
PFD	L-M[1]	5674.43	1920.21	0.87	4.01	5.65	3.30	4.19	4.69	5.37	5.23	4.64	0.58
	B[2]	5605.27	840.11	0.86									
	K-C-V[3]	26386.73	2845.68	0.81									
	M[4]	29473.04	1073.17	0.79									
	S[5]	28952.13	2564.31	0.81									
5D-PFD	L-M[1]	5884.14	967.15	0.90	4.08	3.70	2.18	2.67	3.02	3.68	3.33	2.81	0.59
	B[2]	5855.82	425.01	0.89									
	K-C-V[3]	27179.04	1648.10	0.82									
	M[4]	30264.44	622.65	0.87									
	S[5]	28952.13	1492.18	0.88									

a) 1D = 3.33564×10^{-30} C. m. = 10^{-18} esu cm. Equation: 1 Lippert–Mataga, 2 Bakhshiev, 3 Kawski–Chamma–Viallet, 4 McRae and 5 Suppan.

b) Ground state dipole moment calculated according to Bilot–Kawski, Eq. (18).

c) Excited state dipole moment calculated according to Bilot–Kawski, Eq. (19).

d) Calculated according to Lippert–Mataga correlation, Eq. (13).

e) Calculated according to Bakhshiev correlation, Eq. (14).

f) Calculated according to Kawski–Chamma–Viallet correlation, Eq. (15).

g) Calculated according to McRae correlation, Eq. (16).

h) Calculated according to Suppan correlation, Eq. (17).

i) The angle between the ground state and excited state dipole moment calculated from Eq. (20).

Table 4 Binding energy of PFD and 5D-PFD with active site I and II of HSA

	PFD-site I	5D-PFD-site I	PFD-site II	5D-PFD-site II
ΔE_{ele}	-39.87	-38.53	-27.58	-25.15
ΔE_{vdw}	-28.02	-28.50	-26.65	-27.58
ΔE_{gas}	-67.89	-67.03	-54.23	-52.73
ΔG_{np}	-4.01	-4.09	-3.77	-3.86
ΔG_{pol}	66.50	65.53	43.63	42.60
ΔG_{solv}	62.49	61.44	39.85	38.74
ΔG_{PB}	-5.40	-5.59	-14.38	-13.98

Table 5 The pharmacokinetic parameters (mean ± S.D.) of 5D-PFD in rats following oral and *i.v.* administration at dose of 20 mg/kg and 5 mg/kg (n = 6), respectively.

Formulation	$T_{1/2}$ (mim)	T_{max} (min)	C_{max} (μg/mL)	$AUC_{0\rightarrow\infty}$ (min μg/mL)	Vz/F (mL/kg)	CLz/F (mL/min /kg)	$MRT_{0-\infty}$ (min)
Oral 5D-PFD	29.83±8.01	16.67±2.89	7.27±0.51	473.32±61.01	-	-	46.15±3.00
i.v. 5D-PFD	18.89±1.52	1.00±0.01	10.69±0.93	193.89±17.79	703.83±16.31	25.94±2.48	24.87±1.17

References

[1] S.N. Giri, Q.J. Wang, Y. Xie, J. Lango, D. Morin, S.B. Margolin, A.R. Buckpitt, Pharmacokinetics and metabolism of a novel antifibrotic drug pirfenidone, in mice following intravenous administration, Biopharmaceutics & Drug Disposition, 23 (2002) 203-211.

[2] R.A. Mesa, A. Tefferi, M.A. Elliott, H.C. Hoagland, T.G. Call, G.S. Schroeder, S.Y. Yoon, C.Y. Li, L.A. Gray, S. Margolin, C.C. Hook, A phase II trial of pirfenidone (5-methyl-1-phenyl-2- 1H -pyridone), a novel anti-fibrosing agent, in myelofibrosis with myeloid metaplasia, British Journal of Haematology, 114 (2001) 111-113.

[3] M. Inomata, K. Kamio, A. Azuma, K. Matsuda, N. Kokuho, Y. Miura, H. Hayashi, T. Nei, K. Fujita, Y. Saito, A. Gemma, Pirfenidone inhibits fibrocyte accumulation in the lungs in bleomycin-induced murine pulmonary fibrosis, Respiratory Research, 15 (2014).

[4] S. Leh, O. Vaagnes, S.B. Margolin, B.M. Iversen, T. Forslund, Pirfenidone and candesartan ameliorate morphological damage in mild chronic anti-GBM nephritis in rats, Nephrology Dialysis Transplantation, 20 (2005) 71-82.

[5] S. Tada, M. Nakamuta, M. Enjoji, R. Sugimoto, H. Iwamoto, M. Kato, Y. Nakashima, H. Nawata, Pirfenidone inhibits dimethylnitrosamine-induced hepatic fibrosis in rats, Clinical and Experimental Pharmacology and Physiology, 28 (2001) 522-527.

[6] Q. Shi, X. Liu, Y. Bai, C. Cui, J. Li, Y. Li, S. Hu, Y. Wei, In Vitro Effects of Pirfenidone on Cardiac Fibroblasts: Proliferation, Myofibroblast Differentiation, Migration and Cytokine Secretion, Plos One, 6 (2011).

[7] H. Taniguchi, M. Ebina, Y. Kondoh, T. Ogura, A. Azuma, M. Suga, Y. Taguchi, H. Takahashi, K. Nakata, A. Sato, M. Takeuchi, G. Raghu, S. Kudoh, T. Nukiwa, j. Pirfenidone Clinical Study Grp, Pirfenidone in idiopathic pulmonary fibrosis, European Respiratory Journal, 35 (2010) 821-829.

[8] T. Adachi, Y. Satou, H. Satou, H. Shibata, S. Miwa, Y. Iwase, T. Yamamoto, A. Nishida, N. Masutomi, Assessment of 8-Methosypsoralen, Lomefloxacin, Sparfloxacin, and Pirfenidone phototoxicity in Long-Evans Rats, International Journal of Toxicology, 34 (2015) 16-23.

[9] S. Onoue, Y. Seto, M. Kato, Y. Aoki, Y. Kojo, S. Yamada, Inhalable Powder Formulation of Pirfenidone with Reduced Phototoxic Risk for Treatment of Pulmonary Fibrosis, Pharmaceutical Research, 30 (2013) 1586-1596.

[10] Y. Seto, R. Inoue, M. Kato, S. Yamada, S. Onoue, Photosafety assessments on pirfenidone: Photochemical, photobiological, and pharmacokinetic characterization, Journal of Photochemistry and Photobiology B-Biology, 120 (2013) 44-51.

[11] B. Belleau, J. Burba, EFFECT OF DEUTERIUM SUBSTITUTION IN SYMPATHOMIMETIC AMINES ON ADRENERGIC RESPONSES, Science, 133 (1961) 102-&.

[12] P.W. Manley, F. Blasco, J. Mestan, R. Aichholz, The kinetic deuterium isotope effect as applied to metabolic deactivation of imatinib to the des-methyl metabolite, CGP74588, Bioorganic & Medicinal Chemistry, 21 (2013) 3231-3239.

[13] S.L. Harbeson, R.D. Tung, Deuterium in Drug Discovery and Development, Annual Reports in Medicinal Chemistry, Vol 46, 46 (2011) 403-417.

[14] R.A. Stringer, G. Williams, F. Picard, B. Sohal, O. Kretz, J. McKenna, J.A. Krauser, Application of a Deuterium Replacement Strategy to Modulate the Pharmacokinetics of 7-(3,5-dimethyl-1H-1,2,4-triazol-1-yl)3-(4-methoxy-2-methylphenyl)-2,6-d imethylpyrazolo 5,1-b oxazole, a Novel CRF1 Antagonist, Drug Metabolism and Disposition, 42 (2014) 954-962.

[15] R. Sharma, T.J. Strelevitz, H. Gao, A.J. Clark, K. Schildknegt, R.S. Obach, S.L. Ripp, D.K.

Spracklin, L.M. Tremaine, A.D.N. Vaz, Deuterium Isotope Effects on Drug Pharmacokinetics. I. System-Dependent Effects of Specific Deuteration with Aldehyde Oxidase Cleared Drugs, Drug Metabolism and Disposition, 40 (2012) 625-634.

[16] E. Falb, K. Ulanenko, A. Tor, R. Gottesfeld, M. Weitman, M. Afri, H. Gottlieb, A. Hassner, A highly efficient Suzuki-Miyaura methylation of pyridines leading to the drug pirfenidone and its CD3 version (SD-560), Green Chemistry, 19 (2017) 5046-5053.

[17] Y. Sun, X.H. Liang, Y.Y. Zhao, J. Fan, Solvent effects on the absorption and fluorescence spectra of rhaponticin: Experimental and theoretical studies, Spectrochimica Acta Part a-Molecular and Biomolecular Spectroscopy, 102 (2013) 194-199.

[18] L.S. Liu, Y. Sun, S. Wei, X.Y. Hu, Y.Y. Zhao, J. Fan, Solvent effect on the absorption and fluorescence of ergone: Determination of ground and excited state dipole moments, Spectrochimica Acta Part a-Molecular and Biomolecular Spectroscopy, 86 (2012) 120-123.

[19] Y. Sun, Z. Ji, X.H. Liang, G.B. Li, S.Y. Yang, S. Wei, Y.Y. Zhao, X.Y. Hu, J. Fan, Studies on the binding of rhaponticin with human serum albumin by molecular spectroscopy, modeling and equilibrium dialysis, Spectrochimica Acta Part a-Molecular and Biomolecular Spectroscopy, 87 (2012) 171-178.

[20] C.C. Pye, T. Ziegler, E. van Lenthe, J.N. Louwen, An implementation of the conductor-like screening model of solvation within the Amsterdam density functional package - Part II. COSMO for real solvents(1), Canadian Journal of Chemistry-Revue Canadienne De Chimie, 87 (2009) 790-797.

[21] L.A. Curtiss, K. Raghavachari, P.C. Redfern, J.A. Pople, Assessment of Gaussian-2 and density functional theories for the computation of enthalpies of formation, Journal of Chemical Physics, 106 (1997) 1063-1079.

[22] P.J. Stephens, F.J. Devlin, J.R. Cheeseman, M.J. Frisch, Calculation of optical rotation using density functional theory, Journal of Physical Chemistry A, 105 (2001) 5356-5371.

[23] Y. Sun, W.Q. Wang, H. Cheng, X.S. Jiang, J.J. Wu, Study of the binding and energy transfer of erbium ion with rhaponticin and its pharmacokinetics application, Luminescence, 31 (2016) 1251-1258.

[24] J. Kongsted, A. Osted, K.V. Mikkelsen, P.O. Astrand, O. Christiansen, Solvent effects on the n ->pi(*) electronic transition in formaldehyde: A combined coupled cluster/molecular dynamics study, Journal of Chemical Physics, 121 (2004) 8435-8445.

[25] Y.L. Lin, J.L. Gao, Solvatochromic shifts of the n -> pi* transition of acetone from steam vapor to ambient aqueous solution: A combined configuration interaction QM/MM simulation study incorporating solvent polarization, Journal of Chemical Theory and Computation, 3 (2007) 1484-1493.

[26] J. Catalan, J.P. Catalan, On the solvatochromism of the n <-> pi* electronic transitions in ketones, Physical Chemistry Chemical Physics, 13 (2011) 4072-4082.

[27] E. Buncel, S. Rajagopal, SOLVATOCHROMISM AND SOLVENT POLARITY SCALES, Accounts of Chemical Research, 23 (1990) 226-231.

[28] C. Reichardt, SOLVATOCHROMIC DYES AS SOLVENT POLARITY INDICATORS, Chemical Reviews, 94 (1994) 2319-2358.

[29] E. Lippert, W. Rettig, V. Bonacickoutecky, F. Heisel, J.A. Miehe, PHOTOPHYSICS OF INTERNAL TWISTING, Advances in Chemical Physics, 68 (1987) 1-173.

[30] J. Tomczak, K. Dobek, Coumarin 153 emission thermochromism studied in non-specifically and specifically interacting solvents, Journal of Luminescence, 129 (2009) 884-891.

[31] A. Kawski, On the estimation of excited-state dipole moments from solvatochromic shifts of

absorption and fluorescence spectra, Zeitschrift Fur Naturforschung Section a-a Journal of Physical Sciences, 57 (2002) 255-262.

[32] A. Kawski, P. Bojarski, B. Kuklinski, Estimation of ground- and excited-state dipole moments of Nile Red dye from solvatochromic effect on absorption and fluorescence spectra, Chemical Physics Letters, 463 (2008) 410-412.

[33] (!!! INVALID CITATION !!! {}).

[34] P. Suppan, C. Tsiamis, ABSOLUTE EXCITED-STATE DIPOLE-MOMENTS FROM SOLVATOCHROMIC SHIFTS, Spectrochimica Acta Part a-Molecular and Biomolecular Spectroscopy, 36 (1980) 971-974.

[35] J.T. Edward, CITATION-CLASSIC - MOLECULAR VOLUMES AND THE STOKES-EINSTEIN EQUATION, Current Contents/Engineering Technology & Applied Sciences, (1986) 14-14.

[36] M.H. Abraham, P.L. Grellier, J.L.M. Abboud, R.M. Doherty, R.W. Taft, SOLVENT EFFECTS IN ORGANIC-CHEMISTRY - RECENT DEVELOPMENTS, Canadian Journal of Chemistry-Revue Canadienne De Chimie, 66 (1988) 2673-2686.

[37] M. Ravi, T. Soujanya, A. Samanta, T.P. Radhakrishnan, EXCITED-STATE DIPOLE-MOMENTS OF SOME COUMARIN DYES FROM A SOLVATOCHROMIC METHOD USING THE SOLVENT POLARITY PARAMETER, E(N)(T), Journal of the Chemical Society-Faraday Transactions, 91 (1995) 2739-2742.

[38] P. Suppan, SOLVATOCHROMIC SHIFTS - THE INFLUENCE OF THE MEDIUM ON THE ENERGY OF ELECTRONIC STATES, Journal of Photochemistry and Photobiology a-Chemistry, 50 (1990) 293-330.

[39] V.K. Sharma, P.D. Saharo, N. Sharma, R.C. Rastogi, S.K. Ghoshal, D. Mohan, Influence of solvent and substituent on excited state characterstics of laser grade coumarin dyes, Spectrochimica Acta Part a-Molecular and Biomolecular Spectroscopy, 59 (2003) 1161-1170.

[40] B. Siddlingeshwar, S.M. Hanagodimath, Estimation of first excited singlet-state dipole moments of aminoanthraquinones by solvatochromic method, Spectrochimica Acta Part a-Molecular and Biomolecular Spectroscopy, 72 (2009) 490-495.

[41] M.A. Rauf, J.P. Graham, S.B. Bukallah, M.A.S. Al-Saedi, Solvatochromic behavior on the absorption and fluorescence spectra of Rose Bengal dye in various solvents, Spectrochimica Acta Part a-Molecular and Biomolecular Spectroscopy, 72 (2009) 133-137.

[42] O.A. Adegoke, O.S. Idowu, Solvatochromic behaviours and structure-spectra relationships of 4-carboxyl-2,6-dinitrophenylazohydroxynaphthalenes, Spectrochimica Acta Part a-Molecular and Biomolecular Spectroscopy, 75 (2010) 719-727.

[43] D.A. Case, T.E. Cheatham, T. Darden, H. Gohlke, R. Luo, K.M. Merz, A. Onufriev, C. Simmerling, B. Wang, R.J. Woods, The Amber biomolecular simulation programs, Journal of Computational Chemistry, 26 (2005) 1668-1688.

[44] Y. Sun, Y.Y. Zhao, Enhanced Pharmacokinetics and Anti-Tumor Efficacy of PEGylated Liposomal Rhaponticin and Plasma Protein Binding Ability of Rhaponticin, Journal of Controlled Release, 172 (2013) E82-E83.

Figure 1. Scheme of synthetic route of 5D-PFD

Figure 2. Optimum configuration B3LYP/DZP of PFD (A) and 5D-PFD (B).

Figure 3 Absorption and fluorescence spectra of PFD (A, B) and 5D-PFD (C, D) in different solvents, respectively.

Figure 4. A-C: plots of v_a-v_f vs. $f(\varepsilon, n)$, v_a+v_f vs. $f(\varepsilon, n)$ + 2g(n) and v_a-v_f vs. E_T^N for PFD in different solvents. D-F: plots of v_a-v_f vs. $f(\varepsilon, n)$, v_a+v_f vs. $f(\varepsilon, n)$ + 2g(n) and v_a-v_f vs. E_T^N for 5D-PFD in different solvents.

Figure 5. Frontier orbital of PFD and 5D-PFD calculated by the ADF program.

Figure 6. Effect of metal ions on the absorption spectra of PFD (A) and 5D-PFD (B). NMR titration of metal ions into PFD (C, D) and 5D-PFD (E, F), respectively.

Figure 7. (A, B): Fluorescence spectra of HSA with 1-8 μM PFD and 5D-PFD, respectively. (λ_{ex} = 280 nm). Stern–Volmer (C) and modified Stern–Volmer (D) plots for the PFD–HSA and 5D-PFD–HSA system, respectively.

Figure 8. Binding of PFD (A) and 5D-PFD (B) in the active site I of HSA. Binding of PFD (C) and 5D-PFD (D) in the active site II of HSA. Red dotted lines represented the hydrogen bonding between ligands and HSA.

Figure 9. Mean plasma concentration-time curve of 5D-PFD following oral and i.v. administration at dose of 20 mg/kg and 5 mg/kg in rats.

Synthesis and photophysical properties of deuteration of pirfenidone

Qiuju Yin[a1], Yujie Chen[a1], Meng Zhou[a], Xiangsheng Jiang[a], Junjun Wu[a], Yang Sun[a,b]*

[a] School of Chemical Engineering, Hubei University of Arts and Science, No. 296 Longzhong Road, Xiangyang, Hubei 441053, China

[b] School of Life Sciences, Tsinghua University, Beijing 100084, China

Corresponding author email: sunyang@if.usp.br (Y. Sun),

[1] These authors are co-first author of this work

Highlights

- The deuterium of pirfenidone (5-methyl-1-phenylpyridin-2-one, PFD) by the substitution of hydrogen (H) at C-5 with isotope deuterium (D, 5D-PFD) has been synthesized
- The negative solvatochrom was observed in absorption and fluorescence spectra with increasing solvent polarity, which implied that intermolecular charge transfer involved n→π* transition for both of PFD and 5D-PFD
- A significant propensity for intramolecular charge transfer from the electron-donor methyl and carbonyl group to the amine group as an electron donor has been observed.
- The pyridone ring showed more stability upon binding of unoccupied orbital of metal ions with lone-pair electron of oxygen atom and thus prompted the electronic distribution on phenyl unit.
- The human serum binding and docking results demonstrated that the affinity of 5D-PFD with HSA was lower than that of PFD, and also 5D-PFD may prefer to present free forms in the blood with better efficacy comparing with PFD
- The pharmacokinetic of $T_{1/2}$ values by oral and i.v. administration of 5D-PFD was found around 19 and 30 min.

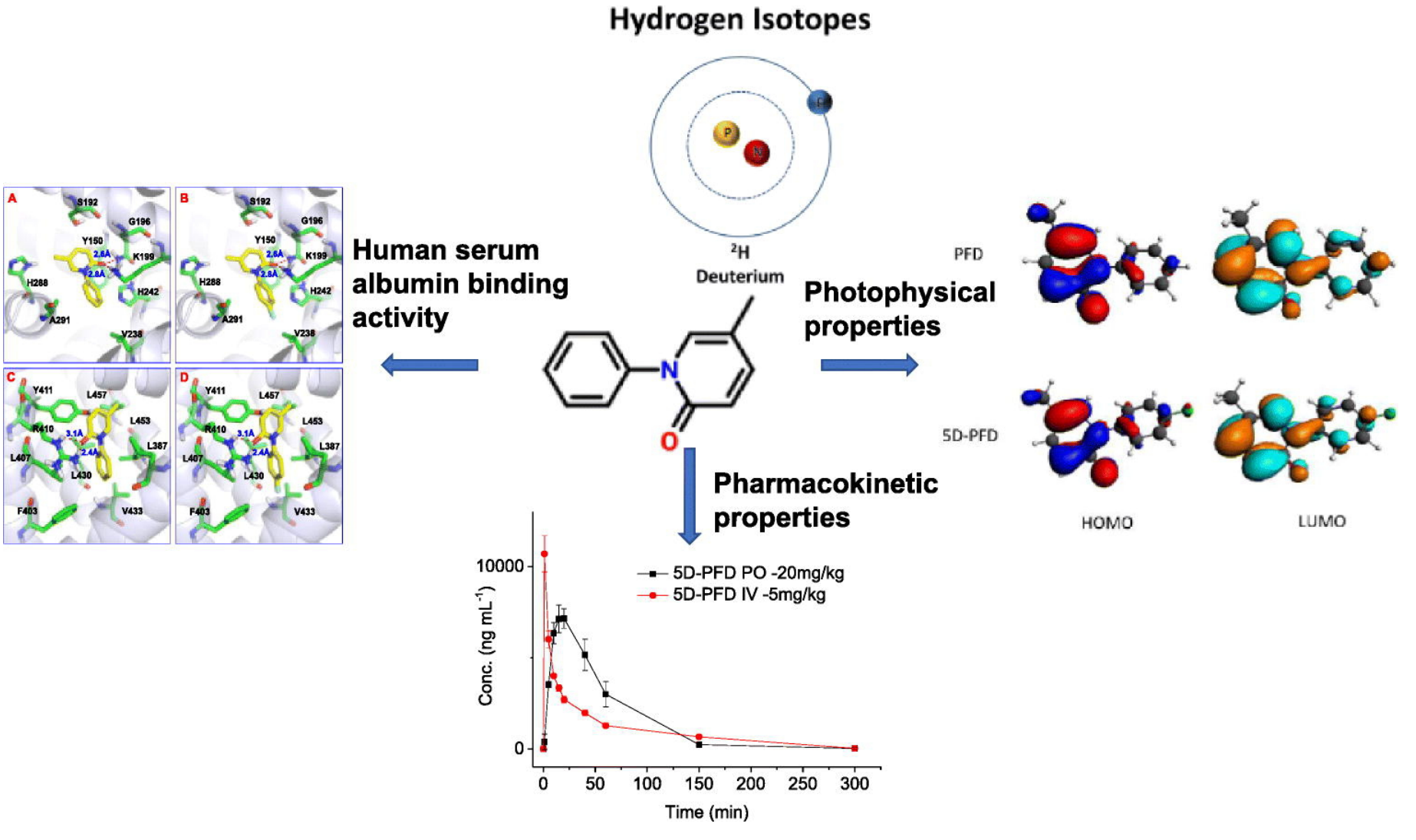

Graphics Abstract

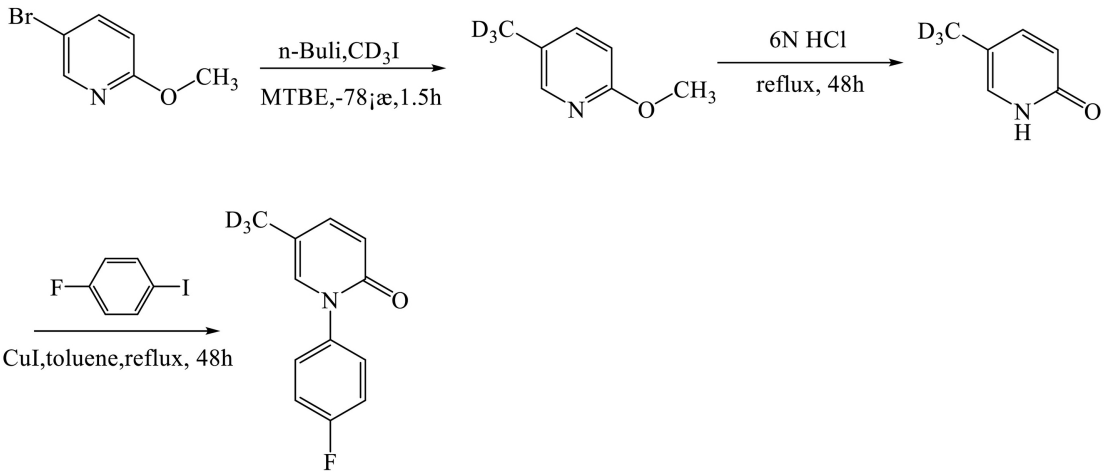
Br
N
O
CH3
n-Buli,CD3I
MTBE,-78¡æ,1.5h
D3C
N
O
CH3
6N HCl
reflux, 48h
D3C
N
H
O
F
I
CuI,toluene,reflux, 48h
D3C
N
O
F

Figure 1

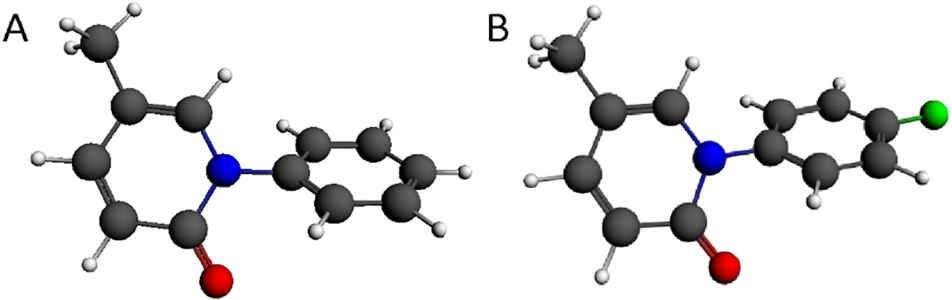

Figure 2

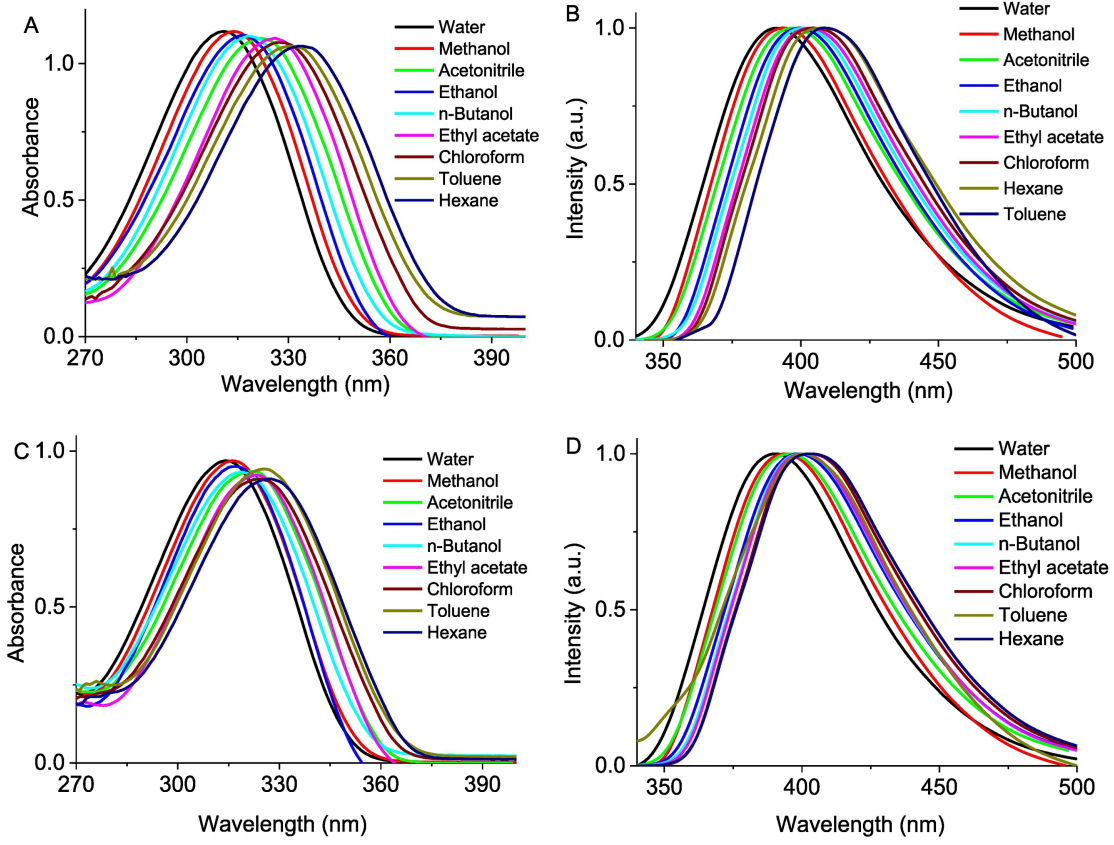
A
Absorbance
Wavelength (nm)
Water
Methanol
Acetonitrile
Ethanol
n-Butanol
Ethyl acetate
Chloroform
Toluene
Hexane
B
Intensity (a.u.)
Wavelength (nm)
C
Absorbance
Wavelength (nm)
D
Intensity (a.u.)
Wavelength (nm)

Figure 3

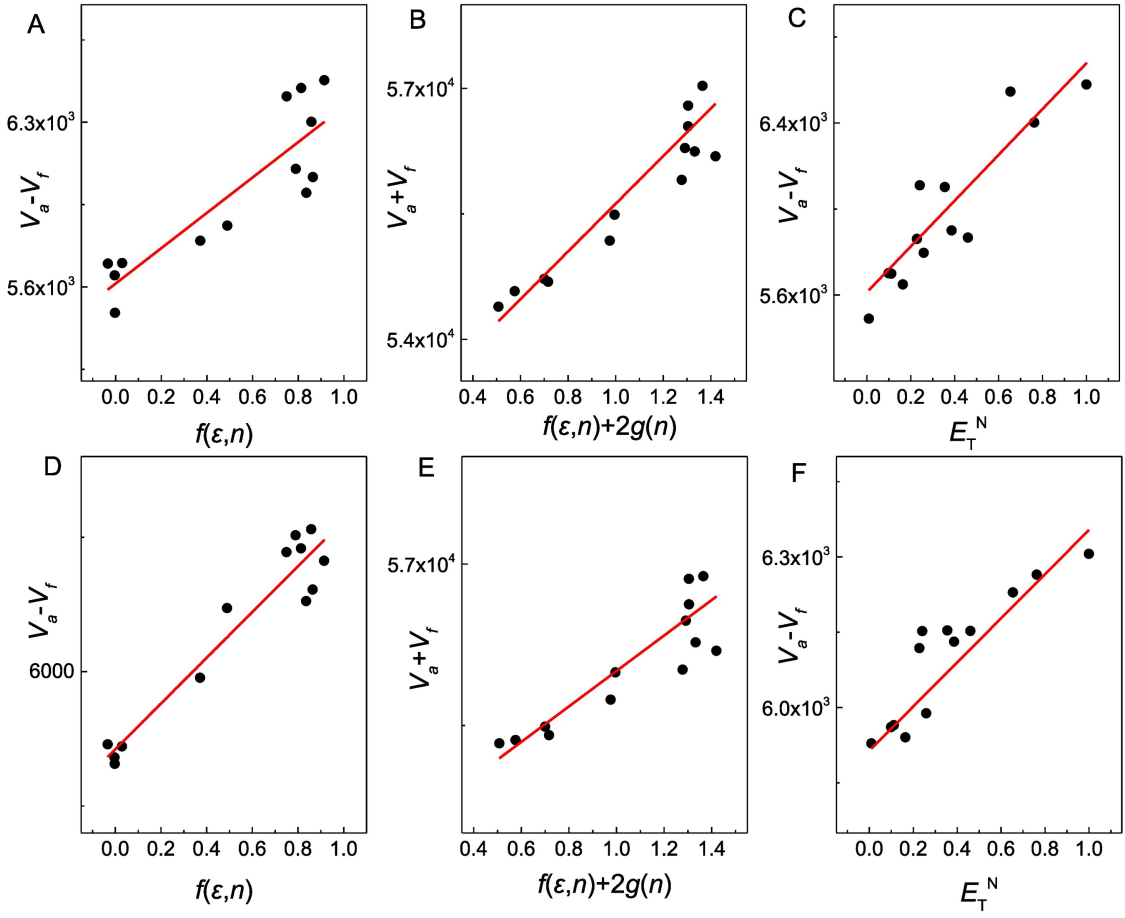
A
B
C
D
E
F
V_a-V_f
V_a+V_f
6.3x10^3
5.6x10^3
5.7x10^4
5.4x10^4
6.4x10^3
6000
6.0x10^3
0.0 0.2 0.4 0.6 0.8 1.0
0.4 0.6 0.8 1.0 1.2 1.4
$f(\varepsilon,n)$
$f(\varepsilon,n)+2g(n)$
E_T^N

Figure 4

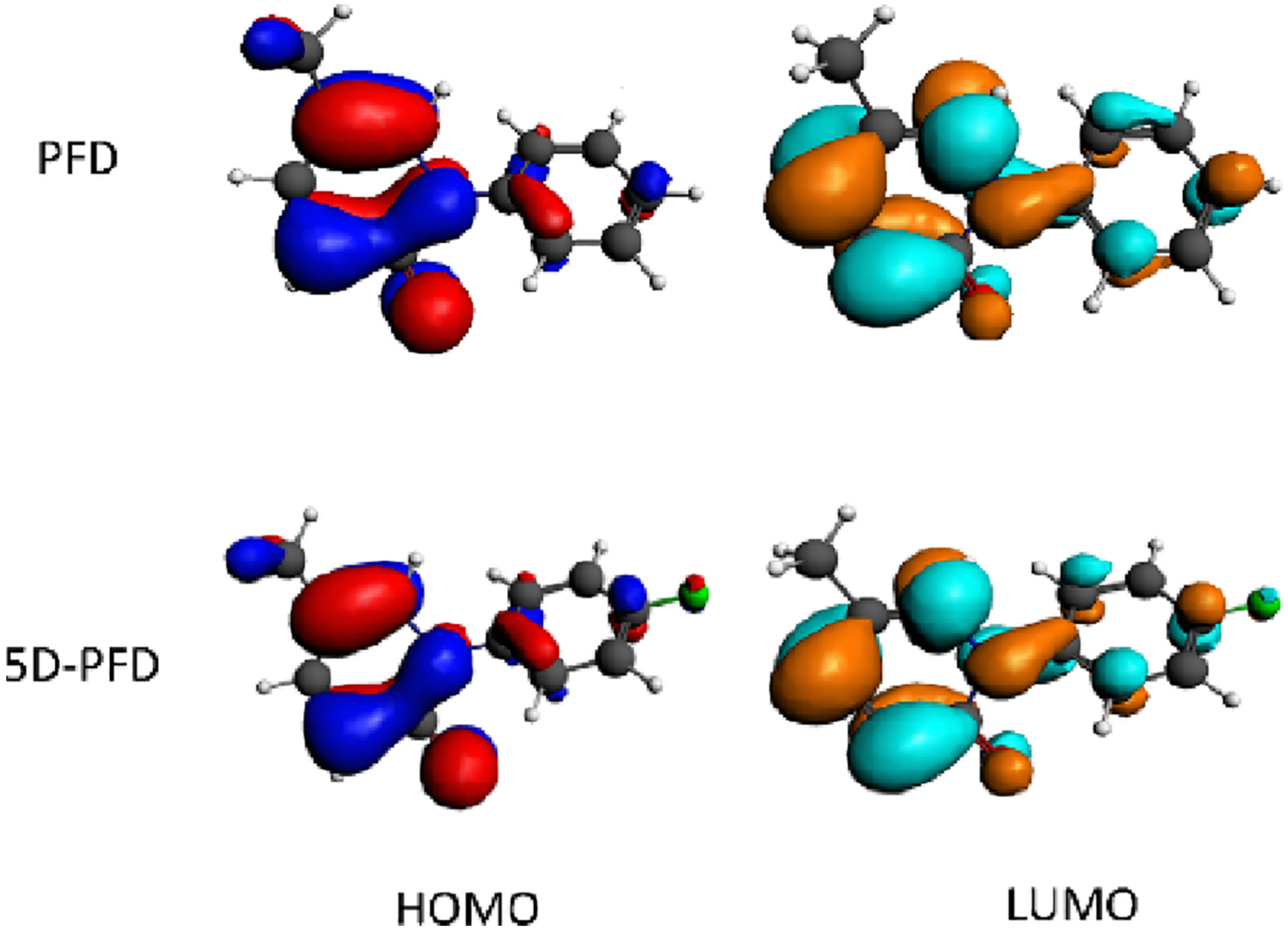

Figure 5

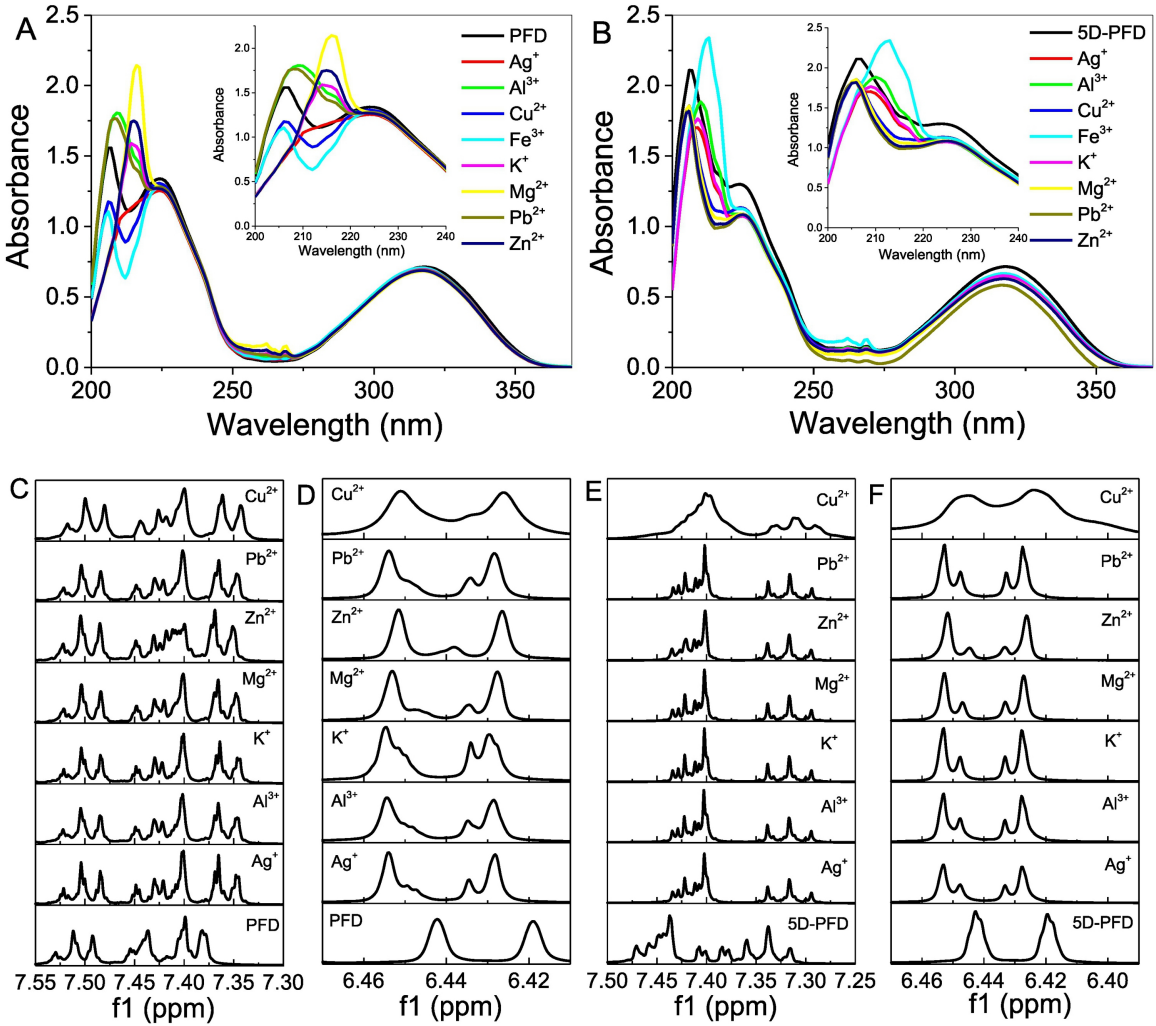
A
Absorbance
Wavelength (nm)
PFD
Ag+
Al3+
Cu2+
Fe3+
K+
Mg2+
Pb2+
Zn2+
B
5D-PFD
C
D
E
F
f1 (ppm)

Figure 6

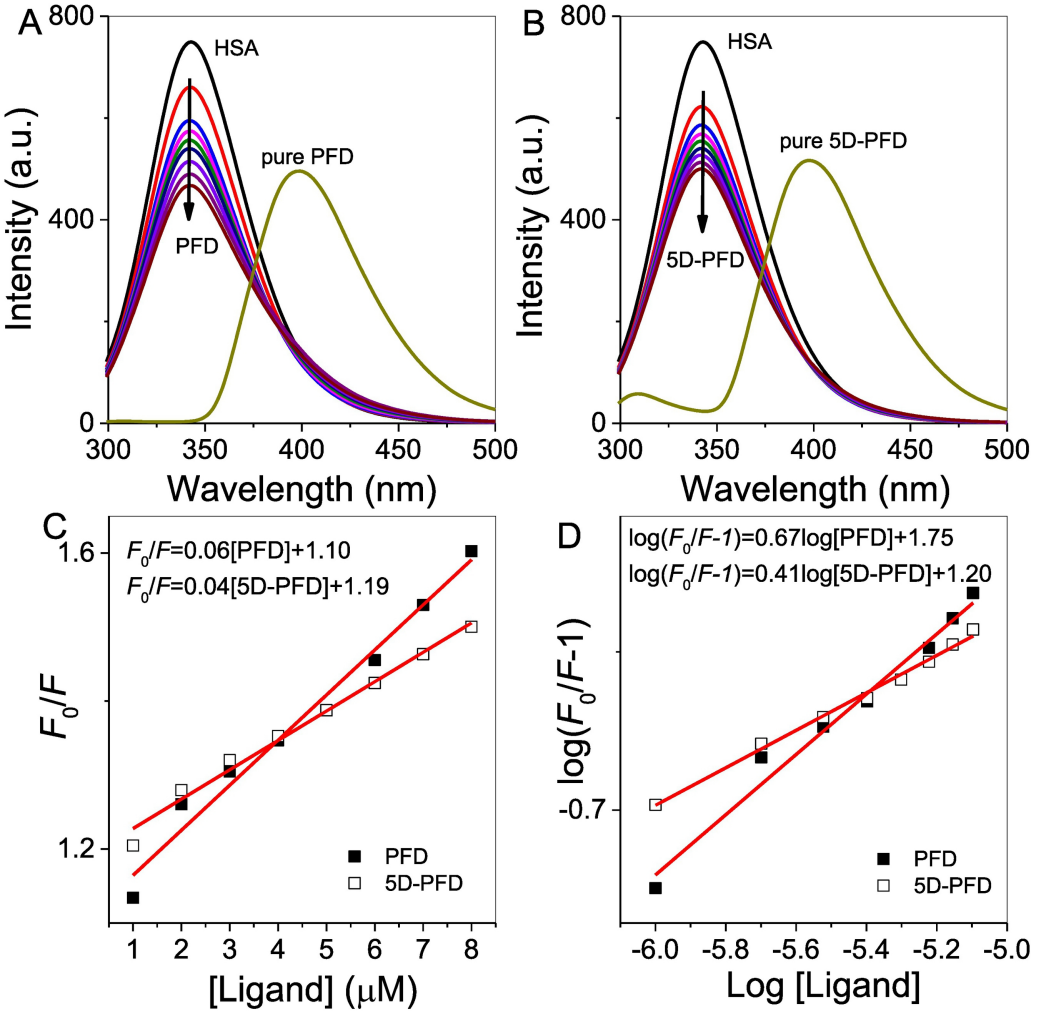
A
800
400
0
Intensity (a.u.)
HSA
pure PFD
PFD
300
350
400
450
500
Wavelength (nm)
B
800
400
0
Intensity (a.u.)
HSA
pure 5D-PFD
5D-PFD
300
350
400
450
500
Wavelength (nm)
C
1.6
1.2
F0/F
F0/F=0.06[PFD]+1.10
F0/F=0.04[5D-PFD]+1.19
PFD
5D-PFD
1
2
3
4
5
6
7
8
[Ligand] (μM)
D
log(F0/F-1)
log(F0/F-1)=0.67log[PFD]+1.75
log(F0/F-1)=0.41log[5D-PFD]+1.20
-0.7
PFD
5D-PFD
-6.0
-5.8
-5.6
-5.4
-5.2
-5.0
Log [Ligand]

Figure 7

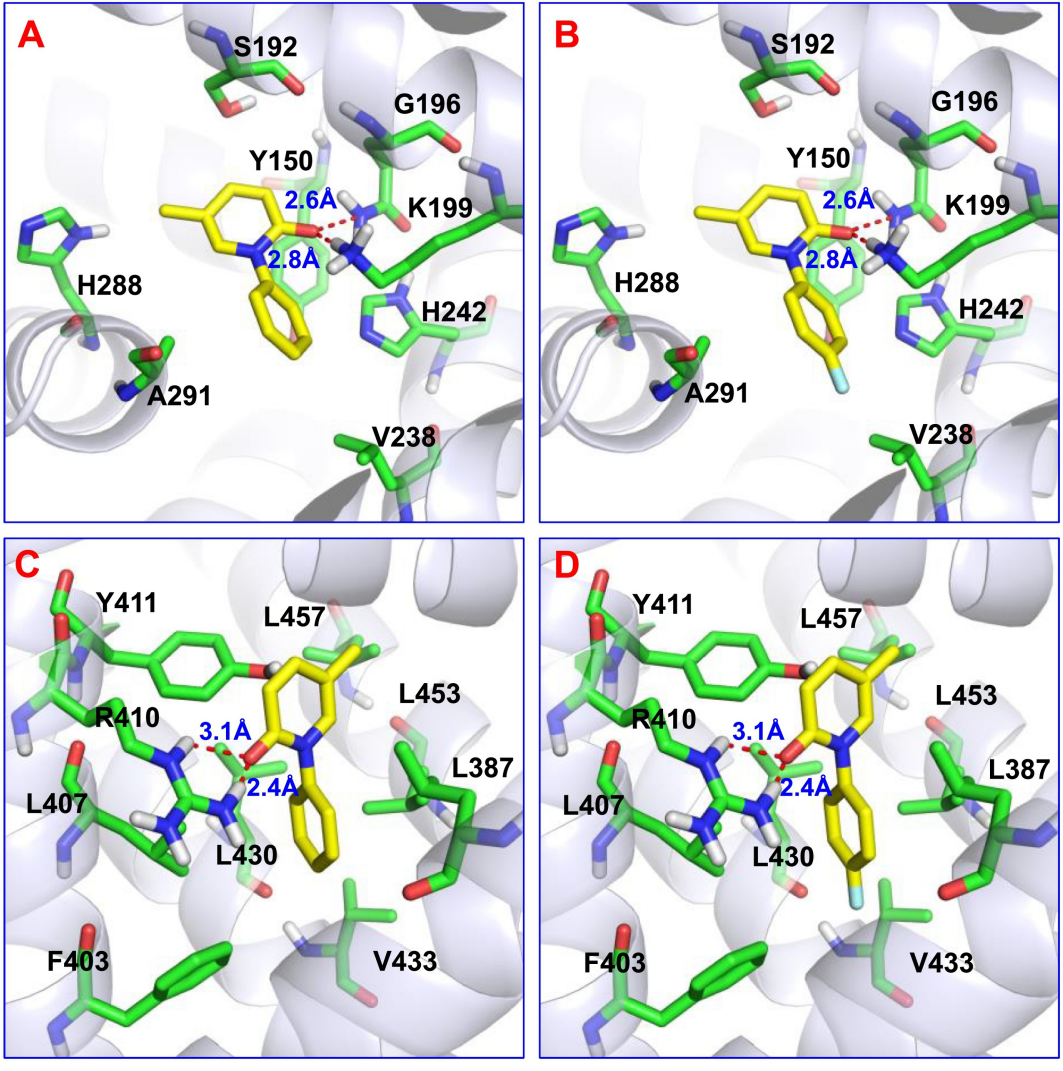
A
S192
G196
Y150
2.6Å
K199
2.8Å
H288
H242
A291
V238
B
S192
G196
Y150
2.6Å
K199
2.8Å
H288
H242
A291
V238
C
Y411
L457
L453
R410
3.1Å
L387
2.4Å
L407
L430
F403
V433
D
Y411
L457
L453
R410
3.1Å
L387
2.4Å
L407
L430
F403
V433

Figure 8

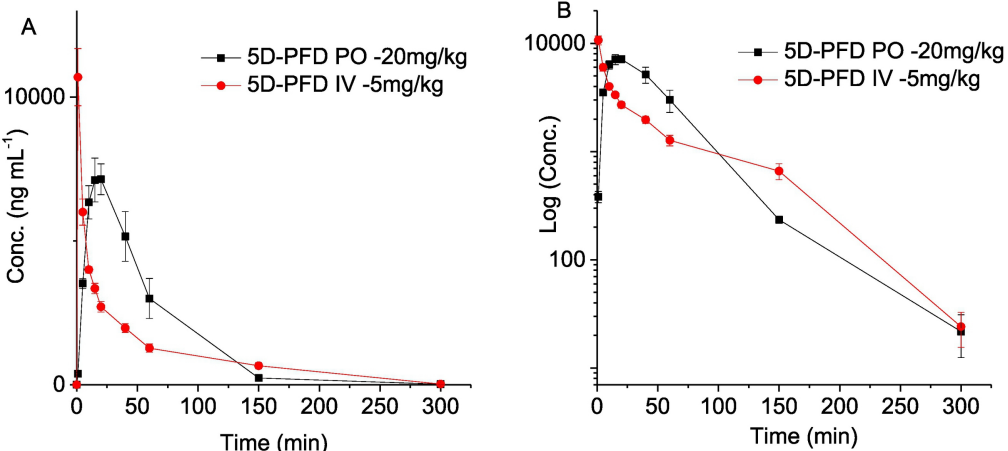
A
5D-PFD PO -20mg/kg
5D-PFD IV -5mg/kg
Conc. (ng mL-1)
10000
0
0
50
100
150
200
250
300
Time (min)
B
5D-PFD PO -20mg/kg
5D-PFD IV -5mg/kg
Log (Conc.)
10000
100
0
50
100
150
200
250
300
Time (min)

Figure 9